

Cross-dimensional Weighting for Aggregated Deep Convolutional Features

Yannis Kalantidis
Yahoo Labs
San Francisco

ykal@yahoo-inc.com

Clayton Mellina
Flickr Vision
San Francisco

clayton@yahoo-inc.com

Simon Osindero
Flickr Vision
San Francisco

osindero@yahoo-inc.com

Abstract

We propose a simple and straightforward way of creating powerful image representations via cross-dimensional weighting and aggregation of deep convolutional neural network layer outputs. We first present a generalized framework that encompasses a broad family of approaches and includes cross-dimensional pooling and weighting steps. We then propose specific non-parametric schemes for both spatial- and channel-wise weighting, that boost the effect of highly active spatial responses and at the same time regulate burstiness effects. We experiment on four public datasets for image search and unsupervised fine-grained classification and show that our approach consistently outperforms the current state-of-the-art by a large margin.

1. Introduction

Visual image search has been evolving rapidly in recent years with hand-crafted local features giving way to learning-based ones. Deep Convolutional Neural Networks (CNNs) were popularized by the seminal work of Krizhevsky *et al.* [18] and have been shown to “effortlessly” improve the state-of-the-art in multiple computer vision domains [28], beating many highly optimized domain-specific approaches. It comes as no surprise that such features, based on deep networks, have recently also dominated the field of visual image search [28, 4, 29, 2, 3].

Many recent image search approaches are based on deep features, *e.g.*, Babenko *et al.* [4, 3] and Razavian *et al.* [28, 29] proposed different pooling strategies for such features and demonstrated state-of-the-art performance in popular benchmarks for *compact* image representations, *i.e.*, representations of up to a few hundred dimensions.

Motivated by these advances, in this paper we present a simple and straightforward way of creating powerful image representations via cross-dimensional weighting and aggregation. We place our approach in a general family of approaches for multidimensional aggregation and weighting and present a specific instantiation that we have thus far

found to be most effective on benchmark tasks.

We base our cross-dimensional weighted features on a generic deep convolutional neural network. Since we aggregate outputs of convolutional layers before the fully connected ones, the data layer can be of arbitrary size [19]. We therefore avoid resizing and cropping the input image, allowing images of different aspect ratios to keep their spatial characteristics intact. After extracting deep convolutional features from the last spatial layer of a CNN, we apply weighting both spatially and per channel before sum-pooling to create a final aggregation. We denote features derived after such cross-dimensional weighting and pooling as *CroW* features.

Our contributions can be summarized as follows:

- We present a generalized framework that sketches a family of approaches for aggregation of convolutional features, including cross-dimensional weighting and pooling steps.
- We propose non-parametric weighting schemes for both spatial- and channel-wise weighting that boost the effect of highly active spatial responses and regulate the effect of channel burstiness respectively.
- We present state-of-the-art results on four public datasets for image search and unsupervised fine-grained classification tasks without any fine-tuning.

With a very small computational overhead, we are able to improve the state-of-the-art in both visual image search and unsupervised fine-grained classification. For the popular *Oxford* [25] and *Paris* [26] datasets, the mean average precision for our *CroW* feature is over 10% higher than the previous state-of-the-art for compact visual representations. Additionally, our features are trivially combined for simple query expansion, enjoying even better performance.

In fine-grained classification, *CroW* features without any fine-tuning beat state-of-the-art unsupervised approaches on the CUB-2011 Birds dataset [36] without the need for any metadata, *e.g.*, bounding boxes, and using simple nearest neighbor search on the full images.

The paper is structured as follows: In Section 2 we present and discuss related works, while in Section 3 we present a general framework for weighted pooling to orient past work and our own explorations. In Section 4 we describe two complimentary feature weighting schemes, and we present experimental results for visual search and fine-grained classification in Section 5. The paper concludes with Section 6.

2. Related work

Until recently, the vast majority of image search approaches were variants of the bag-of-words model [32] and were based on local features, typically SIFT [20]. Successful extensions include soft assignment [26], spatial matching [25], query expansion [6, 5, 1], better descriptor normalization [1], feature selection [35], feature burstiness [13] and very large vocabularies [21]. All the aforementioned strategies perform very well for object retrieval but are very hard to scale, as each image is represented by hundreds of patches, causing search time and memory to suffer.

The community therefore recently turned towards global image representations. Starting from local feature aggregation strategies like VLAD [14] or Fisher Vectors [23] multiple successful extensions have arisen [7, 10, 33], slowly increasing the performance of such aggregated features and closing the gap between global and bag-of-word representations for image search. Triangulation embedding with democratic aggregation [15] was shown to give state-of-the-art results for SIFT-based architectures, while handling problems related to burstiness and interactions between unrelated descriptors prior to aggregation. Recently, Murray and Perronnin [22] generalized max-pooling from bag-of-words to Fisher Vector representations achieving high performance in search as well as classification tasks.

After the seminal work of Krizhevsky *et al.* [18], image search, along with the whole computer vision community, embraced the power of deep learning architectures. Out-of-the-box features from pre-trained Convolutional Neural Networks (CNNs) were shown to effortlessly give state-of-the-art results in many computer vision tasks, including image search [28].

Among the first to more extensively study CNN-based codes for image search were Babenko *et al.* [4] and Razavian *et al.* [28, 29, 2]. They experimented with aggregation of responses from different layers of the CNN, both fully connected and convolutional. They introduced a basic feature aggregation pipeline using max-pooling that, in combination with proper normalization and whitening was able to beat all aggregated local feature based approaches for low dimensional image codes. Gong *et al.* [9] used orderless VLAD pooling of CNN activations on multiple scales and achieved competitive results on classification and search tasks.

Very recently Tolias *et al.* [34] proposed max-pooling over multiple image regions sampled on the final convolutional layer. Their approach achieves state-of-the-art results and is complementary to our cross-dimensional weighting. In another very recent related work, Babenko and Lempit-sky proposed the SPoC features [3], where with slightly different design choices from the pipeline of [4, 29] and sum- instead of max-pooling. As the latter approach is very related to ours, we discuss the differences of the two approaches in the following sections and explain SPoC in terms of the proposed aggregation framework.

3. Framework for Aggregation of Convolutional Features

3.1. Framework Overview

In this section we present a simple and straightforward way of creating powerful image representations. We start by considering a general family of approaches that can be summarized as proceeding through the following steps. Greater details and motivations for these steps will be given in subsequent sections, along with the specific instantiation that we have thus far found to be most effective on benchmark tasks.

1: Perform spatially-local pooling

Sum-pooling or max-pooling over a spatially local neighborhood within each channel of a convolutional layer, with neighborhood size $w \times h$ and stride s . Some limiting cases include: (1) a pooling neighborhood that occupies the full spatial extent of each channel (i.e. global pooling); and (2) a 1×1 pooling neighborhood (effectively not doing pooling at all). After pooling, we have a three-dimensional tensor of activities.

2: Compute spatial weighting factors

For each location (i, j) in the locally pooled feature maps we assign a weight, α_{ij} , that is applied to each channel at that location.

3: Compute channel weighting factors

For each channel k , we assign a weight, β_k that is applied to each location in that channel.

4: Perform weighted-sum aggregation

We apply the previously derived weights location-wise and channel-wise before using a channel-wise sum to aggregate the full tensor of activities into a single vector.

5: Perform vector normalization

The resulting vector is then normalized and power-transformed. A variety of norms can be used here.

6: Perform dimensionality reduction

We then reduce the dimensionality of the normed-vector. PCA is a typical choice here, and we may also choose to perform whitening or other per-dimension

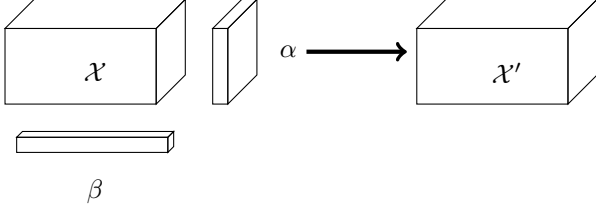


Figure 1: Prior to aggregation, the convolutional features can be weighted channel-wise by a weight vector β and weighted location-wise by a weight matrix α such that $\mathcal{X}'_{kij} = \alpha_{ij}\beta_k\mathcal{X}_{kij}$. The weighted features \mathcal{X}' are summed to derive an aggregate feature.

scalings on entries of the dimensionality reduced vector.

7: Perform final normalization

We then apply a second and final normalization step.

Algorithm 1 summarises these steps as pseudocode.

3.2. Cross-dimensional Weighting

Let $\mathcal{X} \in \mathbb{R}^{(K \times W \times H)}$ be the 3-dimensional *feature* tensor from a selected layer l , where K is the total number of channels and W, H the spatial dimensions of that layer. As mentioned above, the spatial dimensions may vary per image depending on its original size, but we omit image-specific subscripts here for clarity.

We denote the entry in \mathcal{X} corresponding to channel k , at spatial location (i, j) as \mathcal{X}_{kij} . For notational convenience, we also denote the channel-wise matrices of \mathcal{X} as $\mathcal{C}^{(k)}$, where $\mathcal{C}_{ij}^{(k)} = \mathcal{X}_{kij}$. Similarly, we use $\lambda^{(ij)}$ to denote the vector of channel responses at location (i, j) , where $\lambda_k^{(ij)} = \mathcal{X}_{kij}$.

A weighted feature tensor \mathcal{X}' is produced by applying per-location weights, α_{ij} , and per-channel weights, β_k , to feature tensor \mathcal{X} as illustrated in Figure 1:

$$\mathcal{X}'_{kij} = \alpha_{ij}\beta_k\mathcal{X}_{kij} \quad (1)$$

The weighted feature tensor is aggregated by summing per channel. Let *aggregated feature* vector $\mathcal{F} = \{f_1, \dots, f_k\}$ associated with the layer l be the vector of weight-summed activations per channel:

$$f_k = \sum_{i=1}^W \sum_{j=1}^H \mathcal{X}'_{kij} \quad (2)$$

After aggregation, we follow what was shown to be the best practice [28, 2, 29] and L2-normalize \mathcal{F} , then whiten using parameters learnt from a separate dataset and L2-normalize again. We denote the features that are derived from the current framework as *Cross-dimensional Weighted* or *CroW* features.

Algorithm 1: Framework for Aggregation of Convolutional Features

input : 3d feature tensor \mathcal{X} ,

pooling nhood size $w \times h$, stride s , and type p ,
spatial weight generation function, Ω_s ,
channel weight generation function, Ω_c ,
initial norm type, a , and power scaling, b ,
pre-trained whitening parameters \mathbf{W} ,
final feature dimensionality K' ,
final norm type, c

output: K' -dimensional aggregate feature vector

$$\mathcal{G} = \{g_1, \dots, g_{K'}\}$$

- 1 $\tilde{\mathcal{X}} = \text{pool}(\mathcal{X}; w, h, s, p)$ // Initial local pooling
 - 2 $\Omega_s(\tilde{\mathcal{X}}) \rightarrow \alpha_{ij} \forall i, j$ // Spatial weighting
 - 3 $\Omega_c(\tilde{\mathcal{X}}) \rightarrow \beta_k \forall k$ // Channel weighting
 - 4 $f_k = \sum_{i=1}^W \sum_{j=1}^H \alpha_{ij}\beta_k\mathcal{X}_{kij} \forall k$
 - 5 $\hat{\mathcal{F}} = \text{pnorm}(\mathcal{F}; a, b)$ // Normalize and powerscale
 - 6 $\tilde{\mathcal{F}} = \text{PCA}(\hat{\mathcal{F}}; \mathbf{W}, K')$ // dim. reduction and whitening
 - 7 $\mathcal{G} = \text{norm}(\tilde{\mathcal{F}}, c)$ // Normalize again
-

4. Feature Weighting Schemes

In this section we present our non-parametric spatial and channel weighting for Steps 2 and 3 of the framework. We propose a spatial weighting derived from the spatial activations of the layer outputs themselves and a channel weighting derived from channel sparsity.

4.1. Response Aggregation for Spatial Weighting

We propose a method to derive a spatial weighting based on the normalized total response across all channels. Let $\mathcal{S}' \in \mathbb{R}^{(W \times H)}$ be the matrix of aggregated responses from all channels *per spatial location*, which we compute by *summing* feature maps $\mathcal{C}^{(k)}$:

$$\mathcal{S}' = \sum_k \mathcal{C}^{(k)}. \quad (3)$$

After normalization and power-scaling we get aggregated spatial response map \mathcal{S} , whose value at spatial location (i, j) is given by:

$$\mathcal{S}_{ij} = \left(\frac{S'_{ij}}{\left(\sum_{m,n} S'_{mn} \right)^{1/a}} \right)^{1/b}, \quad (4)$$

After computing the 2d spatial aggregation map \mathcal{S} for feature \mathcal{X} , we can apply it independently on every channel, setting $\alpha_{ij} = \mathcal{S}_{ij}$ and using α_{ij} as in Eqn 1.

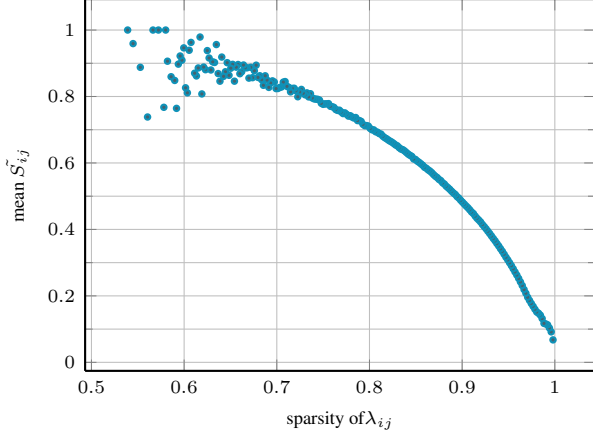


Figure 2: Mean \tilde{S}_{ij} plotted against channel sparsity at the corresponding location.

We experimented with different norms for normalizing the aggregate responses \mathcal{S}' , *i.e.*, L1, L2, *inf*, power normalization with $a = 0.5$ [24]. We found that image search performance remains very high in all cases and the differences are very small, usually less than 0.01 in mAP. We therefore choose to use the L2 norm and $b = 1$ for our spatial aggregation maps, before applying them to the features.

We visualize highly weighted spatial locations in Figure 3 with images from the *Paris* [26] dataset. Our spatial weighting boosts features at locations with salient visual content and down weights non-salient locations. Notably, similar visual elements are boosted under our weighting despite large variation in lighting and perspective.

In Figure 2 we show the relationship between our spatial weights S_{ij} and the sparsity of the channel responses $\lambda^{(ij)}$. We compute the spatial weight S_{ij} of every location in the *Paris* dataset and normalize each by the maximum spatial weight for the image in which it occurs, which we denote \tilde{S}_{ij} . The mean \tilde{S}_{ij} for each level of channel sparsity at the corresponding location is plotted as cyan in Figure 2.

It can be seen that our spatial weighting tends to boost locations for which multiple channels are active relative to other spatial locations of the same image. This suggests that our spatial weighting is a non-parametric and computationally cheap way to favor spatial locations for which features co-occur while also accounting for the strength of feature responses. We speculate that these locations are more discriminative as there are combinatorially more configurations at mid-ranges of sparsity.

4.2. Sparsity Sensitive Channel Weighting

We now propose a method to derive a channel weighting based on the sparsity of feature maps. We expect that similar images will have similar occurrence rates for a given feature. For each channel k we find \mathcal{Q}_k , the proportion of

Step	SPoC [3]	<i>uCroW</i>	<i>CroW</i>
1: local pooling	none	max	max
2: spatial weighting	centering prior	uniform	SW
3: channel weighting	uniform	uniform	SSW
4: aggregation	sum	sum	sum

Table 1: The pooling and weighting steps for three instantiations of our aggregation framework, *i.e.*, the proposed *CroW*, the simplified *uCroW* and SPoC [3]. SW refers to the spatial weighting presented in 4.1, while SSW to the sparsity sensitive channel weighting presented in Section 4.2.

non-zero responses, and compute the *per-channel sparsity*, Ξ_k , as:

$$\Xi_k = 1 - \mathcal{Q}_k, \quad (5)$$

where $\mathcal{Q} = \frac{1}{WH} \sum_{ij} \mathbb{1}[\lambda^{(ij)} > 0]$. In Figure 4 we visualize the pair-wise correlation of the vectors of channel sparsities $\Xi \in \mathbb{R}^K$ for images in the query-set of the *Paris* dataset. The query-set for the *Paris* dataset contains 55 images total, 5 images each for 11 classes of Paris landmarks. We order the images by class. It is apparent that channel sparsities Ξ are highly correlated for images of the same landmark and less correlated for images of different landmarks. It appears that the sparsity pattern of channels contains discriminative information.

Since we sum-pool features $\lambda^{(ij)}$ over spatial locations when we derive our aggregated feature, channels with frequent feature occurrences are already strongly activated in the aggregate feature. However, infrequently occurring features could provide important signal if, for example, the feature consistently occurs though only a small number of times in images of the same class. Motivated by this insight, we devise a channel weighting scheme similar to the concept of *inverse document frequency*. That is, we boost the contribution of rare features in the overall response by using the per-channel weight, \mathcal{I}_k , defined as:

$$\mathcal{I}_k = \log \left(\frac{K\epsilon + \sum_h \mathcal{Q}_h}{\epsilon + \mathcal{Q}_k} \right), \quad (6)$$

where ϵ is a small constant added for numerical stability.

Our sparsity sensitive channel weighting is also related to and motivated by the notion of intra-image visual burstiness [13]. Channels with low sparsity correspond to filters that give non-zero responses in many image regions. This implies some spatially recurring visual elements in the image, that were shown to negatively affect matching [13]. Although we don't go as far as [15] and try to learn a "democratic" matching kernel, our sparsity sensitive weights do down-weight channels of such bursty convolutional filters.

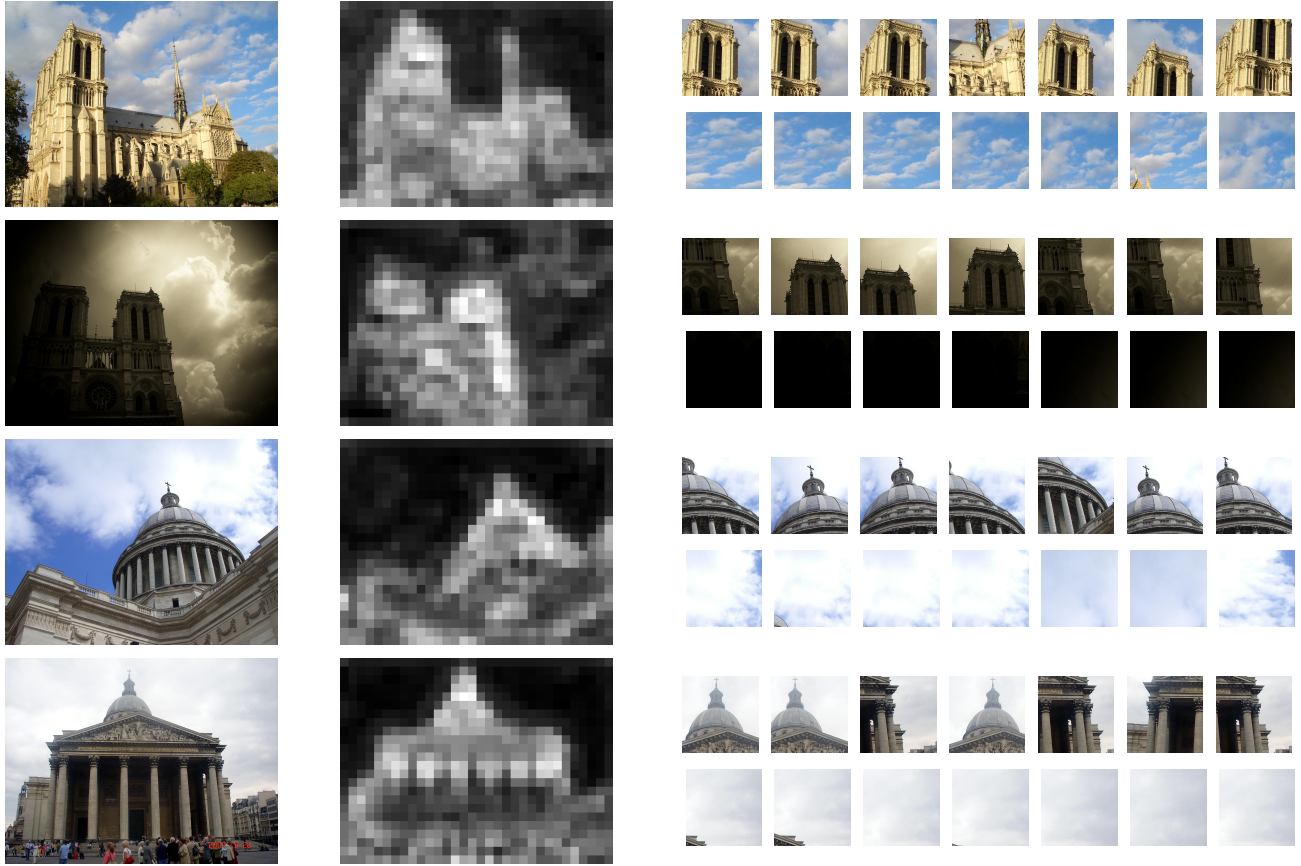


Figure 3: Visualization of spatial weighting by aggregate response. On the left we show original images in the *Paris* dataset along with their spatial weights. On the right we visualize the receptive fields of the 7 highest weighted locations and the 7 lowest weighted locations for each image. The top two images are of Notre Dame and the bottom two are of the Panthéon.

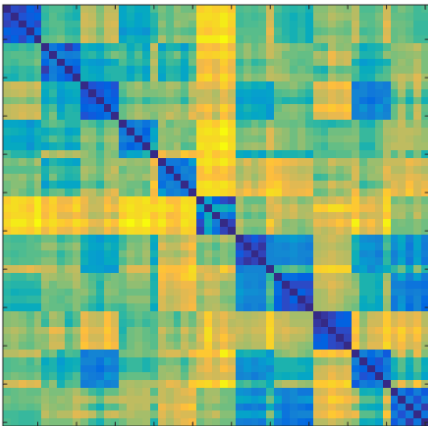


Figure 4: The correlation of channel-wise sparsity for the 55 images in the query-set of the *Paris* dataset. Images are sorted by landmark class in both dimensions.

4.3. Discussion

Using the framework described in Section 3, we can explain different approaches in terms of its pooling, weighting and aggregation steps; we illustrate some interesting cases in Table 1. For example, approaches that aggregate the output of a max-pooling layer of the convolutional neural network are essentially performing max-pooling in Step 1.

Uniform weighting. If we further uniformly set both spatial and channel weights and then perform sum-pooling per channel we end up with a simpler version of *CroW* features, that we denote as *uniform CroW* or *uCroW*.

Relation to SPoC [3] features. SPoC [3] can be described in terms of our framework as illustrated in Table 1. *CroW* and SPoC features differ in their spatial pooling, spatial weighting, and channel weighting. For the first spatially-local pooling step, *CroW* (and *uCroW*) max-pool (we are essentially using the outputs of the last pooling layer of the deep convolutional network rather than the last convolutional one as in SPoC). SPoC uses a centering prior

for spatial weighting to boost features that occur near the center of the image, whereas we propose a spatial weighting derived from the spatial activations of the layer outputs themselves. Lastly, SPoC uses a uniform channel weighting, whereas we propose a channel weighting derived from channel sparsity. We demonstrate improvements for each of these design choices in Section 5.

5. Experiments

5.1. Evaluation Protocol

5.1.1 Datasets

We experiment on four publicly available datasets. For image search we report results on *Oxford* [25] and *Paris* [26], further combining them with the *Oxford100k* [25] dataset as distractors. We also present results on the *Holidays* [12] dataset. For fine-grained classification we report results on the *CUB200-2011 Birds* dataset. We choose not to use any of the extra metadata (e.g., bounding boxes or part annotations) provided.

5.1.2 Evaluation Metrics

For image search experiments on *Oxford*, *Paris* and *Holidays* we measure mean average precision (mAP) over all queries. We use the evaluation code provided by the authors and the cropped versions of the queries. For *Birds* we measure accuracy through simple nearest neighbor search and we report the percentage of queries that return an image of the correct species as their nearest neighbor. We use the train and test splits for our experiment and query the train image set with each image from the test set.

For deep neural networks we use Caffe¹ [16] and the publicly available pre-trained models for VGG16 [31]. As usual with Caffe, we zero-center the input image by *mean pixel subtraction*.

In all cases, table rows including citations present results reported in the cited papers.

5.1.3 Query Expansion

One can trivially use simple query expansion techniques [6] with *CroW* features. Given the ranked list of database images by ascending distance to the query, we sum the aggregated feature vectors of the top M results, L2-normalize and re-query once again. Despite its simplicity, we show that this consistently improves performance, although it does come at the cost of one extra query.

¹<http://caffe.berkeleyvision.org/>

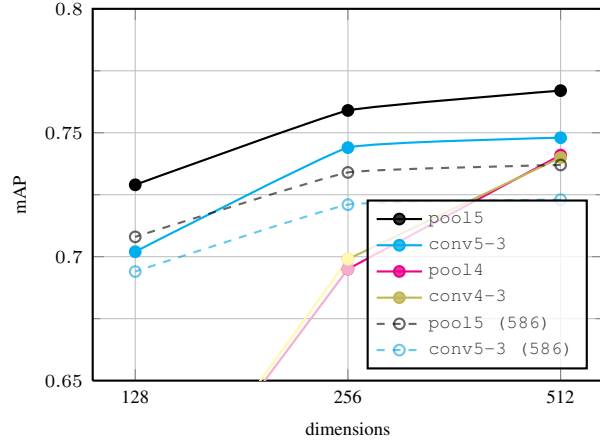


Figure 5: Mean average precision on Paris. Different lines denote *uCroW* features from the corresponding layers of VGG16. Solid lines denote that the original image size is kept, while for dashed lines the images were resized to 586×586 as in [3]. Both *conv4-3* and *pool14* layers have very poor performance in low dimensions, with 0.58 mAP for $d = 128$. SPoC features [3] correspond to the dotted cyan line.

5.2. Preliminary Experiments

Image size and layer selection. In Figure 5 we investigate the performance of *uCroW* features when aggregating responses from different layers of the network.

Our *CroW* features are in essence similar to the very recently proposed SPoC features of [3], but have some different design choices that make them more generic and powerful. Firstly, SPoC features are derived from the VGG19 model while our *uCroW* features are derived from the VGG16 model². Secondly, we do not resize the input image to 586×586 as in [3] and instead keep it at its original size. SPoC is therefore equivalent to the dotted cyan line in Figure 5.

Choosing the last pooling and convolutional layers of the network significantly improves performance over the fourth, especially as the final dimension decreases. Moreover, the *pool15* layer consistently outperforms *conv5-3*, showing that max pooling in Step 1 is indeed beneficial.

Regarding image size, we see that keeping the original size of the images is another factor that contributes to higher performance.

Effect of the final feature dimensionality. In Figure 6 we present mAP on *Paris* when varying the dimensionality of the final features. We present results for all weight-

²As [3] was published only a few days before the deadline, we didn't have time to reproduce their exact features and results using VGG19. We however experiment on the same datasets and show that our *uCroW* features performs much better even using a smaller deep network.

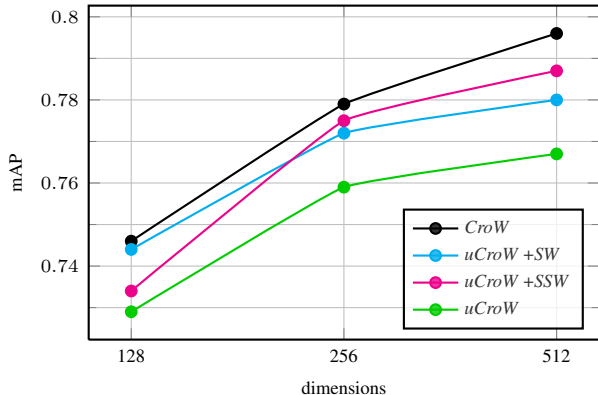


Figure 6: Mean average precision on *Paris* when varying the dimensionality of the final features.

ing combinations of the proposed approach. *uCroW* refers to uniform or no weighting. *uCroW* +SW refers to using the only the spatial weighting of Section 4.1 on top of *uCroW*, *uCroW* +SSW to using the sparsity sensitive channel weighting of Section 4.2 on top of *uCroW*, while *CroW* refers to our complete approach with both weighting schemes. As we see, the *uCroW* +SSW combination is affected more by dimensionality reduction than the rest. This can be interpreted as an effect of the subsequent dimensionality reduction. When calculating the sparsity sensitive weights all dimensions are taken into account, however, in the final reduced vector many of those were discarded.

Notes on max-pooling. In preliminary experiments we also tested max-pooling instead of sum pooling for feature aggregation. Consistently with [3] we found it to be always inferior to sum-pooling when whitening was used. Interestingly, max pooling performs better than sum-pooling in the non-whitened space, but mAP without whitening the features is way inferior (sometimes more than 10% less) in all datasets tested.

Whitening. We learn the whitening parameters from a separate set of images. In Table 2 we present results on the *Paris* dataset when using 3 other datasets for whitening: the semantically related *Oxford* dataset, the *Holidays* dataset and the larger *Oxford100k* dataset. As we reduce the dimensionality, we see overfitting effects for the case where we learn on *Oxford* and this comes as no surprise: as dimensions are reduced, more dimensions that correspond to buildings are kept when we learn the reduction parameters on a semantically similar dataset like *Oxford*.

To be directly comparable with related works, we learn the whitening parameters on *Oxford* when testing on *Paris* and vice versa, as accustomed. We use the *Oxford100k* dataset for whitening in all other cases, *i.e.*, *Holidays* and *Birds*.

d		Oxford	Holidays	Oxford100k
512	<i>uCroW</i>	0.767	0.735	0.770
	<i>CroW</i>	0.796	0.785	0.801
256	<i>uCroW</i>	0.759	0.731	0.734
	<i>CroW</i>	0.779	0.739	0.740

Table 2: Mean average precision on *Paris* when learning the whitening parameters on *Oxford*, *Holidays* and *Oxford100k* for different values of d .

Method	d	Paris	+Oxf100k
<i>uCroW</i>	512	0.767	0.695
<i>CroW</i>	512	0.796	0.710
R-MAC [34]	512	0.830	0.757
Razavian <i>et al.</i> [29]	256	67.0	—
R-MAC [34]	256	0.729	0.601
<i>uCroW</i>	256	0.759	0.672
<i>CroW</i>	256	0.779	0.678
<i>uCroW</i>	128	0.729	0.628
<i>CroW</i>	128	0.746	0.632
<i>CroW</i> + QE	128	0.827	0.750
<i>CroW</i> + QE	256	0.850	0.785
<i>CroW</i> + QE	512	0.855	0.797
Tolias <i>et al.</i> [33]	—	0.770	—
Total Recall II [5]	—	0.805	0.710
Mikulik <i>et al.</i> [21]	—	0.824	0.773

Table 3: Mean average precision on *Paris* against the state-of-the-art for different values of d . QE denotes query expansion with the top $M = 10$ results. The rightmost column presents results when augmenting the *Paris* dataset with the 100k distractors from *Oxford100k*.

5.3. Image Search

In Tables 3, 4 and 5 we present comparisons of our approach with the state-of-the-art in image search on *Paris*, *Oxford* and *Holidays*, respectively. Both *uCroW* and *CroW* consistently outperform all other aggregated methods for different representation sizes, apart from R-MAC [34] that exhibits very high performance for *Oxford* in 512 dimensions. When further combining our approach with query expansion, we get even better results, that compare to (or surpass in *Paris*) far more sophisticated approaches like [21, 5, 33] that are based on local features and include spatial verification steps.

Although our approach is consistently better, the performance gap between *CroW* and the state-of-the-art is smaller in *Holidays*, where it outperforms the best competing method by about 3 and 5% for $d = 256, 512$, respectively.

Method	d	Oxford	+Oxf100k
Tr. Embedding [15]	1024	0.560	0.502
Neural Codes [4]	512	0.435	0.392
<i>uCroW</i>	512	0.666	0.629
R-MAC [34]	512	0.668	0.616
<i>CroW</i>	512	0.682	0.632
Neural Codes [4]	256	0.435	0.392
Razavian <i>et al.</i> [29]	256	0.533	0.489
SPoC [3]	256	0.531	0.501
R-MAC [34]	256	0.561	0.470
<i>uCroW</i>	256	0.635	0.586
<i>CroW</i>	256	0.654	0.593
Tr. Embedding [15]	128	0.433	0.353
Neural Codes [4]	128	0.433	0.384
<i>uCroW</i>	128	0.580	0.505
<i>CroW</i>	128	0.592	0.516
<i>CroW</i> + QE	256	0.692	0.655
<i>CroW</i> + QE	512	0.722	0.678
Tolias <i>et al.</i> [33]	–	0.804	0.750
Total Recall II [5]	–	0.827	0.767
Mikulik <i>et al.</i> [21]	–	0.849	0.795

Table 4: Mean average precision on *Oxford* against the state-of-the-art for different values of d . QE denotes query expansion with the top $M = 10$ results. The rightmost column presents results when augmenting the *Oxford* dataset with the 100k distractors from *Oxford100k*.

Method	d	mAP
Tr. Embedding [15]	1024	0.720
Tr. Embedding [15]	512	0.700
Gong <i>et al.</i> [4]	512	0.783
<i>uCroW</i>	512	0.839
<i>CroW</i>	512	0.849
Tr. Embedding [15]	256	0.657
Razavian <i>et al.</i> [29]	256	0.716
Neural Codes [4]	256	0.749
SPoC [3]	256	0.802
<i>uCroW</i>	256	0.815
<i>CroW</i>	256	0.831

Table 5: Mean average precision on *Holidays* against the state-of-the-art for different values of d .

5.4. Unsupervised Fine-grained Classification

The state-of-the-art on fine-grained classification has advanced rapidly during the last few years, with many approaches either training on or mining object parts [30, 17, 27]. We are mostly interested in fully unsupervised classification, *i.e.*, approaches that do not require bounding boxes or parts for either training or testing and therefore do not

Method	d	Accuracy (%)
<i>CroW</i>	128	34.2
GMP [22]	256	17.0
<i>CroW</i>	256	47.5
Iscen <i>et al.</i> [11]	4K	31.9
Gavves <i>et al.</i> [8]	—	53.6
Simon <i>et al.</i> [30]	—	53.8
<i>uCroW</i>	512	50.2
<i>uCroW</i> +SSW	512	53.9
<i>uCroW</i> +SW	512	55.5
<i>CroW</i>	512	56.5

Table 6: Accuracy for unsupervised fine-grained classification on CUB-2011 Birds dataset.

include in our comparisons part-based approaches [17, 27] that require bounding boxes or parts for training.

Simon *et al.* [30] start from a pre-trained CNN and discover part detectors in a supervised as well as unsupervised way. In their recent paper, Gavves *et al.* [8] propose learning *alignments* of parts of objects using just the overall shape. They use object detectors as voters to generate object confidence saliency maps and a bundle of color Fisher Vectors for representation.

We report results on the *Birds* dataset against the state-of-the-art in Table 6. As this is a different application, we report results for all variants of our approach. We see that our weighting approaches boost performance significantly, both independently and jointly. It is worth noting that the highest performing competitors have very computationally heavy training and testing phases [30] or further require feature fusion [8]. Our approach is training- and parameter-free and independent in the number of classes.

6. Conclusions

In this paper we outline a generalized framework for aggregated deep convolutional features with cross-dimensional weighting and which encompasses recent related works such as [3]. We propose simple, non-parametric weighting schemes for spatial- and channel-wise weighting and provide insights for their behaviour by visualizing and studying the distributional properties of the layer output responses. Using this approach, we report results that consistently and significantly outperform the state-of-the-art in image search and unsupervised fine-grained classification. We also intent to soon update our results and report performance when combining our approach with the very recently published R-MAC [34] approach and max pool regions in multiple scales before summing.

There are several promising directions for future work. Given the success of our spatial and channel weighting

schemes, one might consider the possibility of *learning* the spatial- and channel-wise weighting schemes to achieve an additional performance boost. Likewise, with sufficient ground truth data, it would be possible to consider fine-tuning the entire end-to-end process within our proposed framework using, say, a rank-based loss.

In the appendix we present some further visualizations, *i.e.*, image regions that contribute to sparse versus non-sparse channels and search results for the Paris dataset.

References

- [1] R. Arandjelovic and A. Zisserman. Three things everyone should know to improve object retrieval. In *CVPR*, 2012. 2
- [2] H. Azizpour, A. S. Razavian, J. Sullivan, A. Maki, and S. Carlsson. From generic to specific deep representations for visual recognition. *arXiv preprint arXiv:1406.5774*, 2014. 1, 2, 3
- [3] A. Babenko and V. Lempitsky. Aggregating deep convolutional features for image retrieval. *arXiv preprint arXiv:1408.5093*, 2015. 1, 2, 4, 5, 6, 7, 8
- [4] A. Babenko, A. Slesarev, A. Chigorin, and V. Lempitsky. Neural codes for image retrieval. In *ECCV*, 2014. 1, 2, 8
- [5] O. Chum, A. Mikulik, M. Perdoch, and J. Matas. Total recall II: Query expansion revisited. In *CVPR*, 2011. 2, 7, 8
- [6] O. Chum, J. Philbin, J. Sivic, M. Isard, and A. Zisserman. Total recall: Automatic query expansion with a generative feature model for object retrieval. In *ICCV*, 2007. 2, 6
- [7] J. Delhumeau, P. Gosselin, H. Jegou, and P. Perez. Revisiting the VLAD image representation. In *ACM Multimedia*, 2013. 2
- [8] E. Gavves, B. Fernando, C. G. M. Snoek, A. W. M. Smeulders, and T. Tuytelaars. Local alignments for fine-grained categorization. *IJCV*, 111(2):191–212, January 2015. 8
- [9] Y. Gong, L. Wang, R. Guo, and S. Lazebnik. Multi-scale orderless pooling of deep convolutional activation features. In *ECCV*. 2014. 2
- [10] P.-H. Gosselin, N. Murray, H. Jégou, and F. Perronnin. Revisiting the fisher vector for fine-grained classification. *Pattern Recognition Letters*, 49:92–98, 2014. 2
- [11] A. Iscen, G. Tolia, P.-H. Gosselin, and H. Jegou. A comparison of dense region detectors for image search and fine-grained classification. *TIP*, 24(8):2369–2381, 2015. 8
- [12] H. Jégou, M. Douze, and C. Schmid. Hamming embedding and weak geometric consistency for large scale image search. In *ECCV*, 2008. 6
- [13] H. Jégou, M. Douze, and C. Schmid. On the burstiness of visual elements. In *CVPR*, 2009. 2, 4
- [14] H. Jégou, M. Douze, C. Schmid, and P. Perez. Aggregating local descriptors into a compact image representation. In *CVPR*, 2010. 2
- [15] H. Jégou and A. Zisserman. Triangulation embedding and democratic aggregation for image search. In *CVPR*, 2014. 2, 4, 8
- [16] Y. Jia, E. Shelhamer, J. Donahue, S. Karayev, J. Long, R. Girshick, S. Guadarrama, and T. Darrell. Caffe: Convolutional architecture for fast feature embedding. *arXiv preprint arXiv:1408.5093*, 2014. 6
- [17] J. Krause, H. Jin, J. Yang, and L. Fei-Fei. Fine-grained recognition without part annotations. In *CVPR*. 8
- [18] A. Krizhevsky, I. Sutskever, and G. E. Hinton. Imagenet classification with deep convolutional neural networks. In *NIPS*, 2012. 1, 2
- [19] J. Long, E. Shelhamer, and T. Darrell. Fully convolutional networks for semantic segmentation. *arXiv preprint arXiv:1411.4038*, 2014. 1
- [20] D. Lowe. Local feature view clustering for 3D object recognition. In *CVPR*, 2001. 2
- [21] A. Mikulik, M. Perdoch, O. Chum, and J. Matas. Learning a fine vocabulary. In *ECCV*, 2010. 2, 7, 8
- [22] N. Murray and F. Perronnin. Generalized max pooling. In *CVPR*, 2014. 2, 8
- [23] F. Perronnin, Y. Liu, J. Sanchez, and H. Poirier. Large-scale image retrieval with compressed Fisher vectors. In *CVPR*, 2010. 2
- [24] F. Perronnin, J. Sánchez, and T. Mensink. Improving the fisher kernel for large-scale image classification. In *ECCV 2010*. 2010. 4
- [25] J. Philbin, O. Chum, M. Isard, J. Sivic, and A. Zisserman. Object retrieval with large vocabularies and fast spatial matching. In *CVPR*, 2007. 1, 2, 6
- [26] J. Philbin, O. Chum, J. Sivic, M. Isard, and A. Zisserman. Lost in quantization: Improving particular object retrieval in large scale image databases. In *CVPR*, 2008. 1, 2, 4, 6
- [27] Q. Qian, R. Jin, S. Zhu, and Y. Lin. Fine-grained visual categorization via multi-stage metric learning. In *CVPR*, 2015. 8
- [28] A. S. Razavian, H. Azizpour, J. Sullivan, and S. Carlsson. CNN features off-the-shelf: an astounding baseline for recognition. *arXiv preprint arXiv:1403.6382*, 2014. 1, 2, 3
- [29] A. S. Razavian, J. Sullivan, A. Maki, and S. Carlsson. Visual instance retrieval with deep convolutional networks. *arXiv preprint arXiv:1412.6574*, 2014. 1, 2, 3, 7, 8
- [30] M. Simon, E. Rodner, and J. Denzler. Part detector discovery in deep convolutional neural networks. *arXiv preprint arXiv:1411.3159*, 2014. 8
- [31] K. Simonyan and A. Zisserman. Very deep convolutional networks for large-scale image recognition. *CoRR*, abs/1409.1556, 2014. 6
- [32] J. Sivic and A. Zisserman. Video Google: A text retrieval approach to object matching in videos. In *ICCV*, pages 1470–1477, 2003. 2
- [33] G. Tolia, Y. Avrithis, and H. Jégou. Image search with selective match kernels: Aggregation across single and multiple images. *International Journal of Computer Vision*, pages 1–15, 2015. 2, 7, 8
- [34] G. Tolia, R. Sicre, and H. Jégou. Particular object retrieval with integral max-pooling of CNN activations. *arXiv preprint arXiv:1511.05879*, 2015. 2, 7, 8
- [35] P. Turcot and D. Lowe. Better matching with fewer features: the selection of useful features in large database recognition problems. In *ICCV*, 2009. 2
- [36] C. Wah, S. Branson, P. Welinder, P. Perona, and S. Belongie. The Caltech-UCSD Birds-200-2011 Dataset. Technical report, 2011. 1

A. What are the image regions that contribute to sparse versus non-sparse channels?

To provide further insight into the effect of our sparsity-sensitive channel weights (SSW), we visualize the receptive fields of active locations in channels that our weights boost.

In the right column of Figure 7 we show all receptive fields that are non-zero in (one or more) of the channels with the highest sparsity-sensitive channel weights. As values from these channels are increased before aggregation, our approach gives more weight to CNN outputs that correspond to the image regions shown on the right.

Drawing image regions that correspond to non-zero locations in the two channels with the lowest sparsity sensitive weights gave the complete image in all four examples. Therefore, practically the whole image contributes to such channels.

B. Search Results with *CroW* Features

In the following Figures we present search results for the Paris dataset using the *CroW* features. We present the top-10 results returned with the query image and bounding box shown on the leftmost column. The fact that the queries are cropped is the reason why the image where the query comes from is not always returned in the first position.

In Figure 8 we show the top-10 results for *all 55* queries on the paris dataset using the uncompressed *CroW* features ($d = 512$). **We only have 3 false results in total** for precision@10. This illuminates why query expansion further increases performance: the top ranked results are of high quality.

In Figure 10 we visualize spatial weight maps for the top ten results of a query in $d = 512$ dimensions. The ability of the weight maps to boost locations that contain important objects in the scene despite large variations in scale suggests that *CroW* features have good scale invariance properties.

In Figure 9 we present some interesting results *using just $d = 32$ dimensional features*. They demonstrate the invariance of *CroW* features to viewpoint and lighting variations even after heavy compression.



Figure 7: Left: The sample images from Paris dataset (also shown in Figure 3 in the main text). Right: Image regions corresponding to locations that contribute (are non-zero) to the 10 channels with the highest sparsity-sensitive weights.

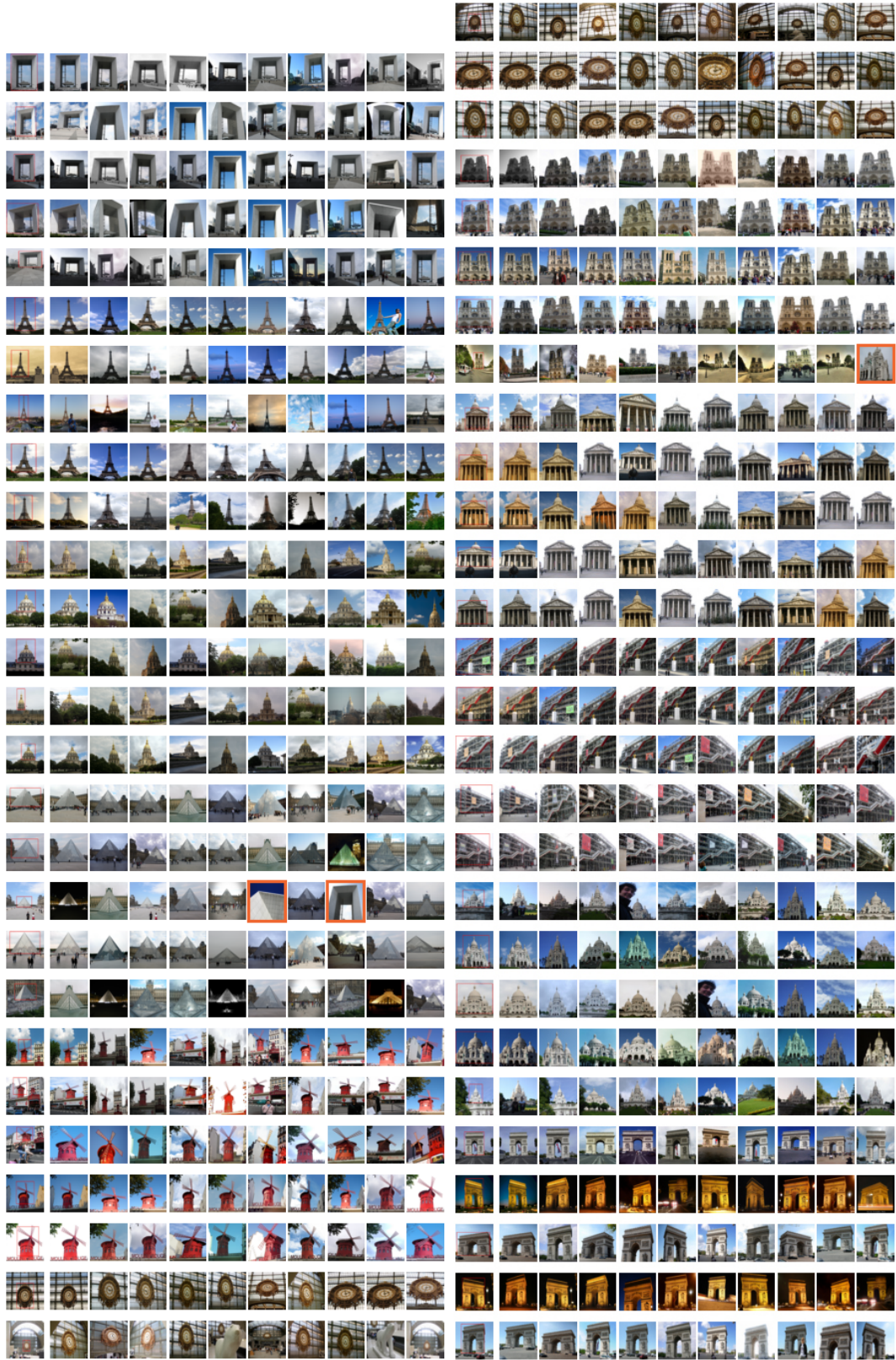


Figure 8: Top-10 results returned for all 55 queries of the Paris dataset, using the 512-dimensional *CroW* features (and no query expansion). The query image is shown on the leftmost place, with the query bounding box marked with a red rectangle. Our features produce just 3 false results in total, which are marked with an orange border.



Figure 9: Sample search results using *CroW* features compressed to just $d = 32$ dimensions. The query image is shown at the leftmost side with the query bounding box marked in a red rectangle.

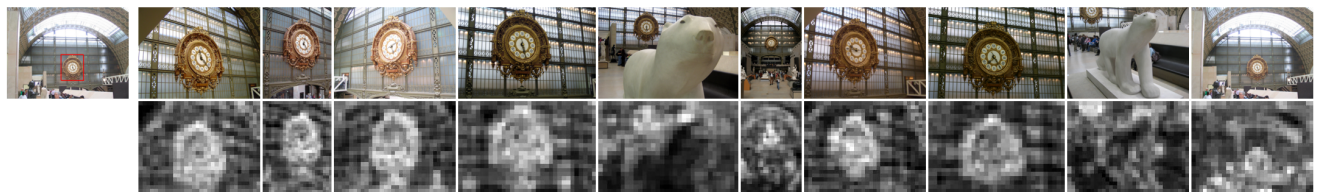


Figure 10: A sample search result using *CroW* features with $d = 512$ dimensions. Below each result is the corresponding spatial weight map. The query image is shown at the leftmost side with the query bounding box marked in a red rectangle.